Article

Fused Double Donor Design with a Cross-Conjugated Dibenzosilin for Dye-Sensitized Solar Cells

Qing Yun Li,[⊥] Ravinder Kaur,[⊥] William E. Meador, Juganta K. Roy, Jerzy Leszczynski, and Jared H. Delcamp*

Cite This: *ACS Omega* 2023, 8, 29234−29246

Read Online

ACCESS | Metrics & More | Article Recommendations | Supporting Information

ABSTRACT: Dye-sensitized solar cells (DSCs) can provide a clean energy solution to growing energy demands. In order to have devices of high performance, sensitizers that are able to absorb in the near-infrared region (NIR) are needed. Stronger electron donors are needed for intramolecular charge-transfer sensitizers to access longer wavelength photons. Thus, two novel organic dyes with a cross-conjugated dibenzosilin double donor design are studied herein. The double donor delocalizes multiple filled orbitals across both amine donors due to the fused design that planarizes the donor as observed computationally, which improves intramolecular charge-transfer strength. The dyes are studied via density functional theory (DFT), optical spectroscopy, electrochemistry, and in DSC devices. The studies indicate that the dye design can reduce recombination losses, allowing for improved DSC device performances relative to a single arylamine donor. The reduction in recombination losses is attributed to the six alkyl chains that are incorporated into the donor, which offer good surface protection.
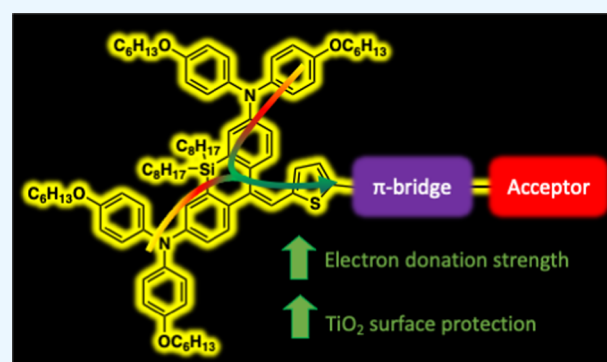
INTRODUCTION

The need for renewable energy sources is growing.[1] Dye-sensitized solar cells (DSCs) are a suitable renewable energy option that convert solar energy to electric energy.[2,3] DSCs are affordable to fabricate, electronically tunable, and efficient in low-light conditions.[2,4−7] In a working DSC, the TiO$_2$-bound photosensitizer is photoexcited in order to inject an electron into the conduction band (CB) of TiO$_2$. The electron then travels via an external circuit to the counter electrode. At the counter electrode, the electron is collected by a redox shuttle (RS), which then returns the electron to the oxidized photosensitizer in order to complete the circuit. In a DSC, the design of the photosensitizer is crucial. A desirable dye is able to harvest light panchromatically from the visible region to the near-infrared region (NIR, >700 nm).[8,9] Several strategies have been utilized to achieve panchromatic spectral activity from sensitizers including concerted companion dyes,[10−12] pyridyl ruthenium-based sensitizers,[13−17] and a variety of chromophore motifs.[18−20] Furthermore, reaching the NIR is critical in order to utilize the vast amount of low-energy photons beyond the visible region (~40%) that are given off by the sun.[3,8,21] Beyond broad and low energy absorption, sensitizers should also exhibit sufficiently high molar absorptivities, efficient electron injection, a strong anchoring group, good surface orientation to minimize aggregation, low back electron-transfer rates between TiO$_2$ and the oxidized dye, and high molecular stability.[9]

Various donor design strategies can be employed in order to increase DSC efficiencies,[9] including bulky donor designs such as on porphyrin[20,22] or amine scaffolds.[23−26] We propose that a greater number of donors strategically positioned on a dye could increase the donation strength within intramolecular charge-transfer (ICT) dyes and thus allow for deeper absorption into the NIR region. Literature has previously reported two dyes, **D9** and **D11**, which were studied in order to examine the effects of cross-conjugation.[27] However, the **D11** dye design did not include a fused donor system resulting in one of the donors being twisted out of plane with the π-system of the acceptor due to steric repulsion. Thus, the data was inconclusive with respect to the impact of the cross-conjugation strategy (Figure 1). Similarly, a series of **TK** dyes and dye **BF3b** were designed and synthesized previously based on fluorene donors, which give intriguing optoelectronic properties (Figure 1).[28,29] However, in our hands, several synthetic routes aiming to use designer π-bridges were unsuccessful primarily due to hydrolysis-type reactions yielding fluorenones as an undesired product when fluorene-based
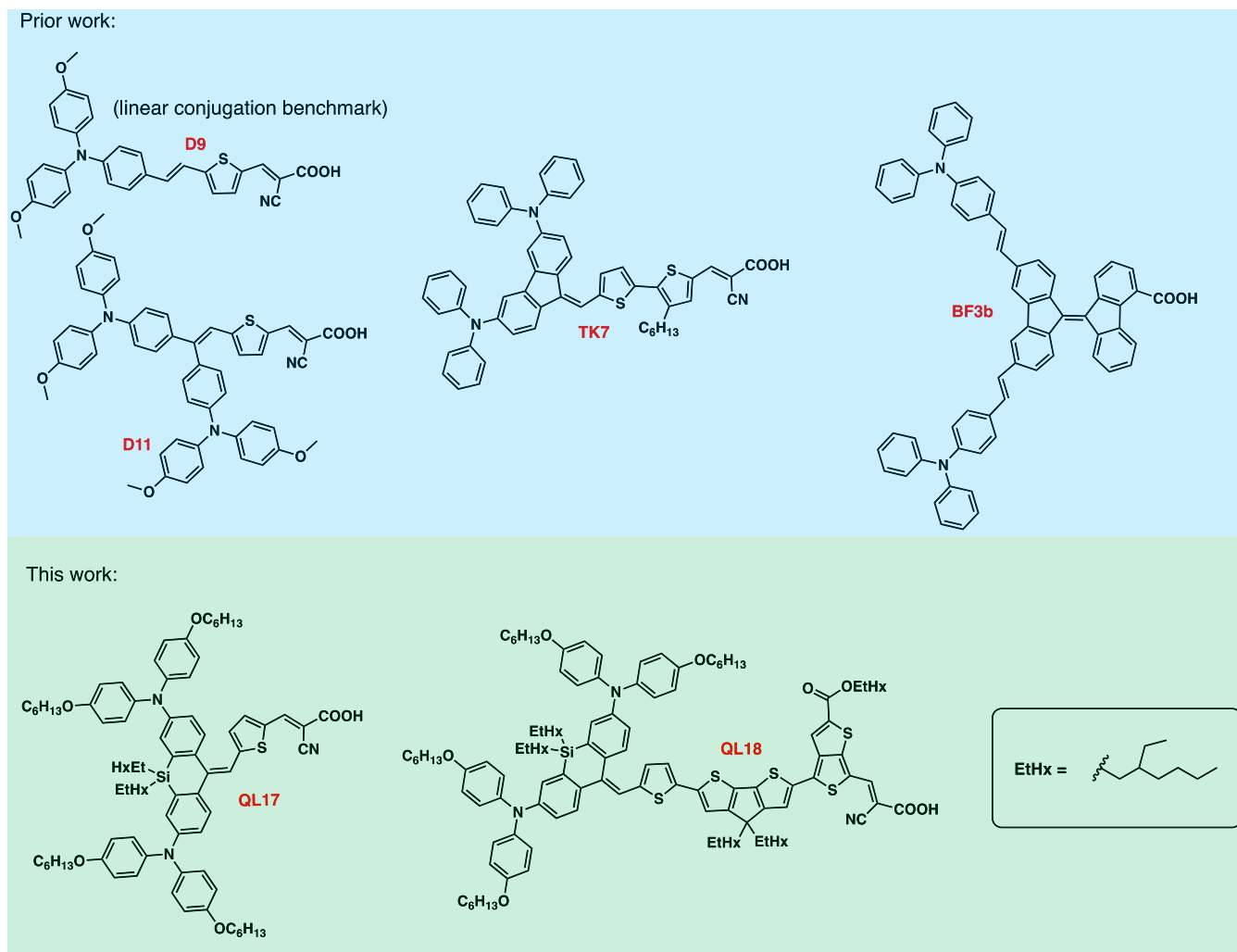
Figure 1. Prior cross-conjugated dyes and the proposed **QL17** and **QL18** dye structures presented in this work.

cross-conjugated donors were used. In this report, a fused cross-conjugated double donor design based on dibenzosilin is used to probe the impact of increased electron density on the donor. The double donor design utilizes two arylamine donor groups that are fused together by a silicon bridge. The amines were employed due to their electron-rich nature and strong donation strength. The silicon atom bridge is used to provide planarity within the donor unit, allowing both amine groups to donate into the π-system. The novel silicon-fused bulky donor also serves to slow recombination events and therefore enhances device performance through the incorporation of multiple large alkyl chains that help insulate the TiO₂ surface.[30−32] A thiophene π-bridge is linked to the donor in order to provide easy synthetic access to cross-coupling reaction manifolds.

Two novel DSC dyes were selected for this study, **QL17** and **QL18** (Figure 1). Both dyes feature the fused double donor, with **QL17** having the thiophene π-bridge linked directly to the electron-withdrawing anchoring group, cyanoacrylic acid (CAA). **QL18** implements a larger π-bridge, which extends conjugation to further red-shift the dye. Specifically, **QL18** utilizes cyclopentadithiophene (CPDT) as part of the π-bridge and 3,4-thienothiophene as an auxiliary acceptor. CPDT is used because it often raises molar absorptivities while

extending conjugation.[33−35] 3,4-thienothiophene is a proaromatic structure that facilitates ICT events at low energies.[36]

■ EXPERIMENTAL SECTION

General Information. All commercially obtained reagents were used as received. Diethyl (thiophen-2-ylmethyl)-phosphonate (**2**) was obtained from Alfa Aesar and used as received. 3,7-dichloro-5,5-bis(2-ethylhexyl)dibenzo[*b*,*e*]silin-10(5*H*)-one (**1**), bis(4-(hexyloxy)phenyl)amine (**4**), and 2-ethylhexyl 4-(6-bromo-4,4-bis(2-ethylhexyl)-4*H*-cyclopenta-[2,1-b:3,4-b']dithiophen-2-yl)-6-formylthieno[3,4-*b*]-thiophene-2-carboxylate (**8**) shown in Scheme 1 were prepared by following literature precedent.[34,37,38] Thin-layer chromatography (TLC) was conducted with Sorbtech silica XHL TLC plates and visualized with UV light. Flash column chromatography was performed with Sorbent Tech P60, 40−63 μm (230−400 mesh). Flash column chromatography was performed using a Teledyne CombiFlash Rf+ system. The silica gel cartridges were purchased from Luknova SuperSep (FC003012, 50 μm). ¹H and ¹³C{¹H} NMR spectra were recorded on a Bruker Avance-400 (400 MHz) instrument and are reported in ppm using solvent as an internal standard (CDCl₃ at 7.26 ppm). Data reported as s = singlet, d = doublet, t = triplet, q = quartet, p = pentet, m = multiplet, br = broad, ap = apparent, dd = doublet of doublets; coupling

Scheme 1. Synthetic Route to QL17 and QL18
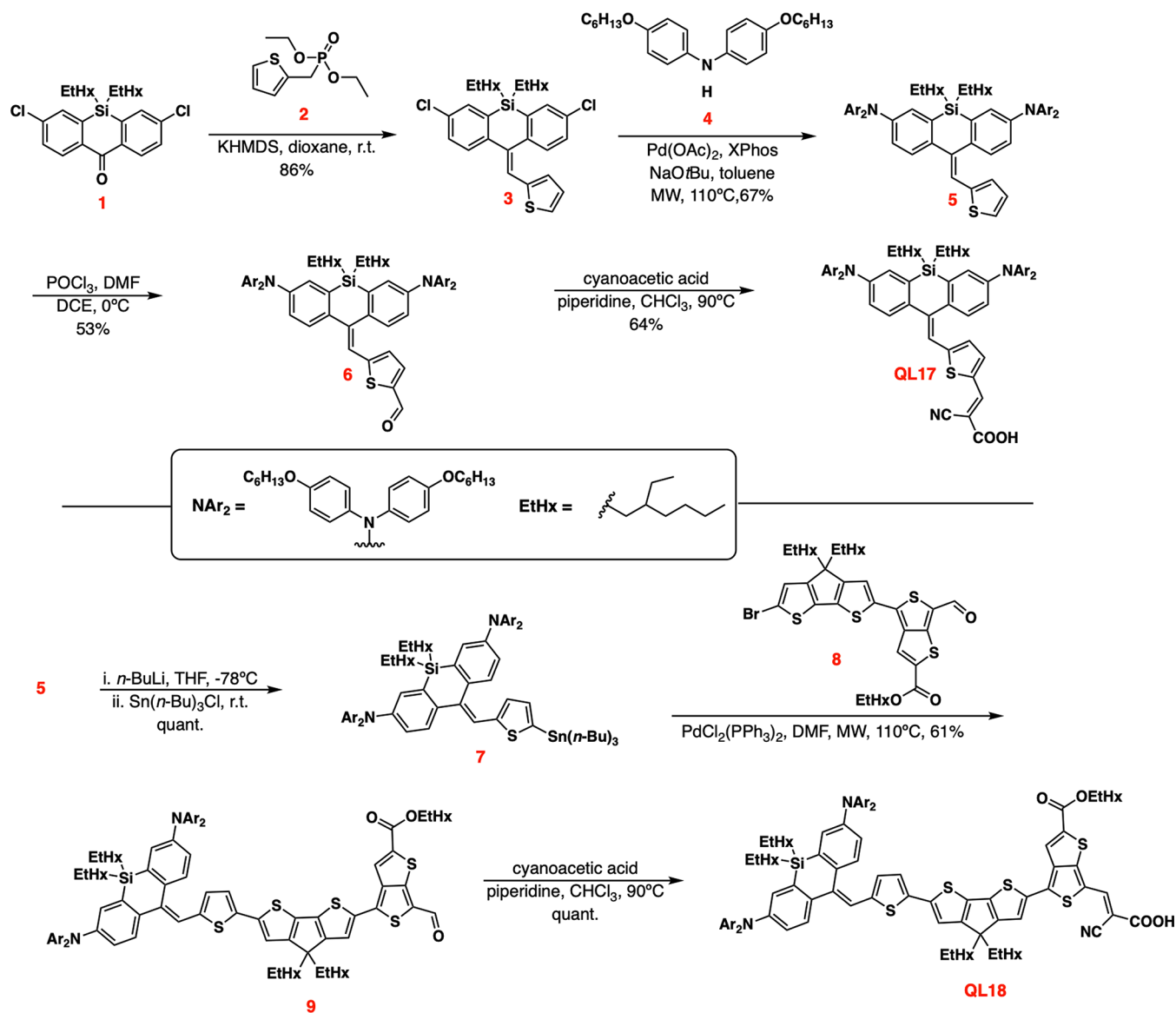
constant(s) in Hz. UV spectra were measured with an AvaSpec-ULS2048-USB2-50 Spectrometer (Pine Research part RRAVSP3), and the light source was a UV/Vis/NIR Light Source (Pine Research part RRAVSP). These two systems were used in conjunction with the AvaSoft8 software program. Curves were fitted with the LOESS function in Igor, which allows for easier data interpretation and comparisons. Cyclic voltammetry curves were measured with a C−H Instruments electrochemical analyzer CHI600E. Tetrabutylammonium hexafluorophosphate (0.1 M in dichloromethane) was used as the electrolyte. The working electrode is glassy carbon, the pseudo-reference electrode is a silver wire, and the counter electrode is platinum. A scan rate of 100 mV/s was used. Ferrocenium/ferrocene is used as an internal standard (taken as 0.70 V vs normal hydrogen electrode (NHE) in dichloromethane (DCM)).[39,40] For electrospray ionization (ESI) high-resolution mass spectrometry (HRMS), a quadruple-TOF system was used to obtain the data both in positive and negative modes with a Waters Synapt HDMS. IR experiments were recorded on a Bruker Alpha FT-IR spectrometer. Microwave synthesis was conducted using a

CEM Discover 1.0 microwave synthesizer with 10 mL CEM glass vials and caps. All microwave reaction conditions included irradiation with 300 W of power, a maximum pressure setting of 150 psi, a maximum ramp time (time to ramp temperature up to reaction temperature) of 5 min, temperature monitoring using a built-in IR sensor, and compressed air cooling after reaction hold time.

Computational Approach. Molecules were drawn in ChemDraw (19.1.0.5) and saved as an MDL Molfile. Molecular geometries of the considered species were then optimized with the MMFF94 force field via Avogadro (1.2.0). Dihedral angles about noncyclic single bonds were set to between 0 and 90° manually to avoid local minima conformations. Accurate geometry optimization was performed sequentially by DFT using Guassian16[41] with the B3LYP[42,43] functional applying the following basis sets: first 3-21G, second 6-31G(d,p),[44,45] and finally 6-311G(d,p).[46] 21 Harmonic vibrational frequencies were computed to confirm that all stationary points on the potential energy surface represent minimum energy structures. Time-dependent DFT (TD-DFT) computations were performed with optimized geometries with

the B3LYP functional and 6-311G(d,p) basis set to compute the vertical transition energies and oscillator strengths.

Synthetic protocols. *3,7-Dichloro-5,5-bis(2-ethylhexyl)-10-(thiophen-2-ylmethylene)-5,10-dihydrodibenzo[b,e]siline (3).* Into a flame-dried flask equipped with a stir bar and flushed with nitrogen, 3,7-dichloro-5,5-bis(2-ethylhexyl)-dibenzo[b,e]silin-10(5H)-one (**1**) (1.00 g, 1.99 mmol) and diethyl(thiophen-2-ylmethyl)phosphonate (**2**) (0.39 mL, 1.99 mmol) were dissolved in dioxane (20 mL). 0.5 M KHMDS in toluene (4.96 mmol, 9.9 mL) was then added dropwise. The reaction was stirred at room temperature and monitored for completion by observing the disappearance of starting material via NMR. Once the reaction was complete, the mixture was then extracted with diethyl ether and water. The organic layer was dried with sodium sulfate and concentrated under reduced pressure. The crude material was purified via silica gel column chromatography with 100% hexanes as the eluent to yield the pure product (**3**) (997 mg, 86%). NMR: ^{1}H NMR (400 MHz, CDCl$_3$) δ 7.70−7.63 (m, 2H), 7.60 (d, J = 8.3 Hz, 1H), 7.55 (s, 1H), 7.37 (dd, J = 8.3 Hz, 1H), 7.24 (dd, J = 8.3 Hz, 1H), 7.12 (d, J = 5.0 Hz, 1H), 6.98−6.86 (m, 3H), 1.60−1.43 (m, 2H), 1.33-.66 (m, 32H) ppm. ^{13}C $\{^1$H$\}$ NMR (400 MHz, CDCl$_3$) δ 147.1, 141.6, 139.9, 139.0, 138.7, 136.6, 133.9, 133.6, 132.9, 132.5, 131.4, 129.5, 129.4, 128.7, 126.7, 126.4, 125.8, 124.6, 35.7, 35.4, 29.0, 28.7, 23.0, 14.2, 10.8, 10.7 ppm. (Note: due to alkane chain stereochemistry, multiple diastereomers are present, which impacts the number of NMR signals observed.) IR (neat, cm^{-1}): 3068, 2956, 2924, 2870, 2856, 1715, 1421, 1100, 695. HRMS ESI (positive mode) m/z calc'd for C$_{34}$H$_{44}$Cl$_2$SSiCs [M + Cs]$^+$ 715.1365, found 715.1331.

5,5-Bis(2-ethylhexyl)-N^3,N^3,N^7,N^7-tetrakis(4-(hexyloxy)-phenyl)-10-(thiophen-2-ylmethylene)-5,10-dihydrodibenzo-[b,e]siline-3,7-diamine (5). Into a flame-dried microwave tube equipped with a stir bar and flushed with nitrogen were added 3,7-dichloro-5,5-bis(2-ethylhexyl)-10-(thiophen-2-ylmethylene)-5,10-dihydrodibenzo[b,e]siline (**3**) (900 mg, 1.54 mmol), bis(4-(hexyloxy)phenyl)amine (**4**) (1.37 g, 3.70 mmol), and sodium *tert*-butoxide (740 mg, 7.71 mmol) in dry toluene (7 mL). The solution was degassed with nitrogen for 10 min. Pd(OAc)$_2$ (35 mg, 0.15 mmol) and XPhos (147 mg, 0.31 mmol) were then added. The reaction was heated to 110 °C in a microwave reactor at 150 psi and 300 W for 1 h. The reaction was monitored by NMR until all of the starting material was observed to be consumed. The mixture was purified via filtering through a pad of silica with 100% diethyl ether as the eluent to remove salts and further purified via silica gel column chromatography with 25% dichloromethane/75% hexanes as the eluent to yield the pure product (**5**) (1.29 g, 67%). NMR: ^{1}H NMR (400 MHz, CDCl$_3$) δ 7.54−7.46 (m, 2H), 7.24−7.20 (m, 1H), 7.16−7.13 (m, 1H), 7.08−6.94 (m, 11H), 6.90−6.77 (m, 11H), 3.93 (t, J = 6.6 Hz, 8H), 1.78, (p, J = 6.7 Hz, 8H), 1.53−1.28 (m, 26H), 1.16−0.88 (m, 28H), 0.77 (at, J = 6.5 Hz, 10H), 0.60 (t, J = 6.7 Hz, 6H) ppm. ^{13}C $\{^1$H$\}$ NMR (400 MHz, CDCl$_3$) δ 155.3, 155.2, 147.3, 146.5, 142.2, 141.6, 141.3, 141.1, 140.9, 137.2, 135.9, 135.1, 130.6, 128.0, 126.5, 126.4, 126.3, 126.1, 125.4, 124.9, 124.5, 122.7, 121.6, 121.3, 115.3, 115.2, 68.4, 35.6, 35.3, 31.8, 29.5, 28.8, 28.8, 28.7, 25.9, 23.1, 22.8, 14.3, 14.2, 10.8 ppm. (Note: due to alkane stereochemistry, multiple diastereomers are present, which impacts the number of NMR signals observed.) IR (neat, cm^{-1}): 2925, 1584, 1502, 1466, 1234, 1166, 1031, 825,

691, 523. HRMS ESI (positive mode) m/z calc'd for C$_{82}$H$_{112}$N$_2$O$_4$SSi [M]$^+$ 1248.8112, found 1248.8119.

5-((3,7-Bis(bis(4-(hexyloxy)phenyl)amino)-5,5-bis(2-ethylhexyl)dibenzo[b,e]silin-10(5H)-ylidene)methyl)-thiophene-2-carbaldehyde (6). Into a flame-dried flask equipped with a stir bar and flushed with nitrogen, **5** (150 mg, 0.12 mmol) was dissolved in dry dichloroethane (0.3 mL) and cooled to 0 °C. N,N-dimethylformamide (DMF) (0.01 mL, 0.13 mmol) was added, and then POCl$_3$ (0.01 mL, 0.13 mmol) was added dropwise. The reaction was stirred for 2 h before monitoring for the disappearance of starting material via TLC. After the starting material was consumed, half-saturated KOH$_{(aq)}$ was added and stirred for an hour. The mixture was then extracted with DCM and saturated KOH$_{(aq)}$. The organics were dried with sodium sulfate and then concentrated under reduced pressure. The crude product was purified via silica gel column chromatography with 50% dichloromethane/50% hexanes as the eluent to yield the pure product (**6**) (81 mg, 53%). ^{1}H NMR (400 MHz, CDCl$_3$) δ 9.79 (s, 1H), 7.55−7.40 (m, 3H), 7.24−7.19 (m, 1H), 7.16−6.97 (m, 11H), 6.91−6.74 (m, 10H), 4.07−3.87 (m, 8H), 1.90−0.53 (m, 78H) ppm. ^{13}C NMR $\{^1$H$\}$ (400 MHz, CDCl$_3$) δ 182.7, 155.6, 155.4, 152.2, 148.2, 147.2, 146.3, 141.1, 141.0, 141.0, 141.0, 137.2, 136.2, 135.1, 134.4, 130.6, 128.7, 126.8, 126.4, 125.8, 125.7, 125.4, 122.1, 120.9, 120.3, 115.4, 115.3, 68.4, 35.6, 35.3, 31.7, 29.5, 28.8, 28.7, 25.9, 23.1, 22.8, 14.3, 14.2, 10.8, 10.8 ppm. (Note: due to alkane chain stereochemistry, multiple diastereomers are present, which impacts the number of NMR signals observed.) IR (neat, cm^{-1}): 3041, 2954, 2925, 2857, 1714, 1661, 1580, 1503, 1467, 1235, 827, 731. HRMS ESI (positive mode) m/z calc'd for C$_{83}$H$_{112}$N$_2$O$_5$SSiCs [M + Cs]$^+$ 1409.7116, found 1409.7161.

(E)-3-(5-((3,7-Bis(bis(4-(hexyloxy)phenyl)amino)-5,5-bis(2-ethylhexyl)dibenzo[b,e]silin-10(5H)-ylidene)methyl)-thiophen-2-yl)-2-cyanoacrylic Acid (QL17). Into a flame-dried pressure flask equipped with a stir bar and flushed with nitrogen was dissolved **6** (37 mg, 0.029 mmol) in chloroform (0.29 mL). Cyanoacetic acid (7 mg, 0.087 mmol) was added, followed by piperidine (0.02 mL, 0.20 mmol). The mixture was degassed with nitrogen for 10 min. The reaction was then allowed to stir at 90 °C for 1 h and monitored by TLC for the consumption of starting material. After the consumption of starting material, the reaction was extracted with dichloromethane and water with a few drops of acetic acid. The organics were dried with sodium sulfate and concentrated under reduced pressure. The crude product was purified via silica gel chromatography with 10% methanol/90% dichloromethane as the eluent to yield the pure product (**QL17**) (25 mg, 64%). ^{1}H NMR (400 MHz, CDCl$_3$) δ 8.15 (br s, 1H), 7.48−7.34 (m, 2H), 7.20−6.60 (m, 23H), 3.90 (t, J = 5.4 Hz, 8H), 2.09−1.60 (m, 18H), 1.49−0.41 (m, 60H) ppm. Aggregation limits good resolution at concentrations needed for a carbon NMR within a reasonable time frame. IR (neat, cm^{-1}): 3372, 3041, 2925, 2214, 1606, 1580, 1503, 1467, 1376, 1236, 827. HRMS ESI (positive mode) m/z calc'd for C$_{86}$H$_{113}$N$_3$O$_6$SSiCs [M + Cs]$^+$ 1476.7174, found 1476.7150.

5,5-Bis(2-Ethylhexyl)-N^3,N^3,N^7,N^7-tetrakis(4-(hexyloxy)-phenyl)-10-((5-(tributylstannyl)thiophen-2-yl)methylene)-5,10-dihydrodibenzo[b,e]siline-3,7-diamine (7). Into a flame-dried flask equipped with a stir bar and flushed with nitrogen, **5** (500 mg, 0.40 mmol) was dissolved in dry tetrahydrofuran (THF, 1.3 mL) and cooled to −78 °C. 2.5 M n-BuLi in hexanes (0.18 mL, 0.44 mmol) was then added dropwise.

Once deprotonation was observed to be complete via NMR by obtaining a reaction sample via a dry pipette and quenching with D_2O; $SnBu_3Cl$ (0.12 mL, 0.44 mmol) was then added, and the reaction was allowed to stir overnight. The reaction was quenched with brine, and the reaction was then extracted with dichloromethane and brine. The organics were dried with sodium sulfate and concentrated under reduced pressure. The crude material was taken forward into the next step without further purification (assumed quantitative). ^1H NMR (400 MHz, $CDCl_3$) δ 7.55 (d, J = 8.4 Hz, 1H), 7.48, (d, J = 8.4 Hz, 1H), 7.23−7.18 (m, 1H), 7.15−7.12 (m, 1H), 7.07−6.94 (m, 12H), 6.86−6.77 (m, 9H), 3.92 (t, J = 6.5 Hz, 8H), 1.82−0.53 (m, 105H) ppm. IR (neat, cm^{-1}): 2924, 1584, 1503, 1463, 1236, 826, 517. HRMS ESI (positive mode) m/z calc'd for $C_{94}H_{139}N_2O_4SSiSn$ [M + H]$^+$ 1540.9280, found 1540.9331.

2-Ethylhexyl-4-(6-(5-((3,7-bis(bis(4-(hexyloxy)phenyl)-amino)-5,5-bis(2-ethylhexyl)dibenzo[b,e]silin-10(5H)-ylidene)methyl)thiophen-2-yl)-4,4-bis(2-ethylhexyl)-4H-cyclopenta[2,1-b:3,4-b']dithiophen-2-yl)-6-formylthieno[3,4-b]thiophene-2-carboxylate (9). Into a flame-dried microwave tube equipped with a stir bar and flushed with nitrogen were added **7** (400 mg, 0.26 mmol) and 2-ethylhexyl-4-(6-bromo-4,4-bis(2-ethylhexyl)-4H-cyclopenta[2,1-b:3,4-b']dithiophen-2-yl)-6-formylthieno[3,4-b]thiophene-2-carboxylate (**8**) (139 mg, 0.17 mmol) in dry DMF (1.7 mL). The solution was degassed with nitrogen for 10 min. $PdCl_2(PPh_3)_2$ (6 mg, 0.01 mmol) was then added. The reaction was heated in a microwave reactor for 1 h at 110 °C, 150 psi, and 300 W. At this point, the reaction was monitored by TLC, and all of the starting material was observed to be consumed. The mixture was extracted with hexanes and water. The organics were concentrated under reduced pressure. The crude product was purified via silica gel chromatography with 50% dichloromethane/50% hexanes as the eluent to yield the pure product (**9**) (209 mg, 61%). ^1H NMR (400 MHz, $CDCl_3$) δ 9.84 (s, 1H), 8.10 (s, 1H), 7.59 (d, J = 8.4 Hz, 1H), 7.48 (d, J = 8.5 Hz, 1H), 7.39 (s, 1H), 7.25−7.22 (m, 1H), 7.15−6.74 (m, 23H), 4.35−4.25 (m, 2H), 3.93 (t, J = 6.6 Hz, 8H), 2.03−0.56 (m, 127H) ppm. ^{13}C NMR (400 MHz, $CDCl_3$) δ 178.7, 162.7, 160.8, 158.8, 155.4, 155.3, 147.6, 146.7, 141.9, 141.7, 141.5, 141.4, 141.3, 141.2, 141.0, 141.0, 140.4, 137.3, 136.2, 135.6, 135.0, 134.6, 133.8, 130.7, 129.5, 126.4, 126.2, 125.3, 123.3, 123.0, 123.0, 122.3, 121.3, 118.2, 115.3, 68.5, 68.4, 54.5, 43.3, 39.0, 35.7, 35.5, 35.5, 35.3, 34.3, 31.8, 30.6, 29.8, 29.5, 29.3, 29.1, 28.9, 28.8, 28.7, 28.7, 27.6, 27.6, 27.4, 25.9, 24.1, 23.1, 23.1, 22.9, 22.9, 22.8, 22.7, 14.3, 14.3, 14.2, 14.2, 14.2, 13.8, 11.2, 10.9, 10.8, 10.0 ppm. (Note: due to alkane stereochemistry, multiple diastereomers are present, which impacts the number of NMR signals observed.) IR (neat, cm^{-1}): 2923, 1714, 1639, 1503, 1457, 1235, 1165, 826, 731. HRMS ESI (positive mode) m/z calc'd for $C_{123}H_{166}N_2O_7S_5Si$ [M]$^+$ 1972.1101, found 1972.1061.

(E)-3-(4-(6-(5-((3,7-Bis(bis(4-(hexyloxy)phenyl)amino)-5,5-bis(2-ethylhexyl)dibenzo[b,e]silin-10(5H)-ylidene)methyl)-thiophen-2-yl)-4,4-bis(2-ethylhexyl)-4H-cyclopenta[2,1-b:3,4-b']dithiophen-2-yl)-2-(((2-ethylhexyl)oxy)carbonyl)-thieno[3,4-b]thiophen-6-yl)-2-cyanoacrylic Acid (QL18). Into a flame-dried pressure flask equipped with a stir bar and flushed with nitrogen was dissolved **9** (100 mg, 0.05 mmol) in chloroform (0.5 mL). Cyanoacetic acid (13 mg, 0.15 mmol) was added, followed by piperidine (0.03 mL, 0.35 mmol). The mixture was degassed with nitrogen for 10 min. The reaction was then allowed to stir at 90 °C for 2 h and was monitored by

TLC. The reaction was then extracted with dichloromethane and water with a few drops of acetic acid. The organics were dried with sodium sulfate and concentrated under reduced pressure. The crude product was purified via silica gel chromatography with 10% methanol/90% dichloromethane as the eluent to yield the pure product (**QL18**) (103 mg, quantitative). ^1H NMR (400 MHz, $CDCl_3$) δ 8.29 (br s, 1H), 8.06 (br s, 1H), 7.57 (d, J = 8.5 Hz, 1H), 7.50−7.39 (m, 2H), 7.24−7.19 (m, 1H), 7.17−6.63 (m, 23H), 4.28 (ap br s, 2H), 3.98−3.78 (m, 8H), 1.95 (ap br s, 2H), 1.83−0.50 (m, 125H) ppm. Aggregation limits good resolution at concentrations needed for a carbon NMR within a reasonable time frame. IR (neat, cm^{-1}): 2926, 2209, 1505, 1239. HRMS ESI (positive mode) m/z calc'd for $C_{126}H_{167}N_3O_8S_5SiCs$ [M + Cs]$^+$ 2172.0214, found 2172.0339.

Device Fabrication. Chenodeoxycholic acid (CDCA) was purchased from Chem-Impex International. Photoanodes and platinum counter electrodes were prepared as described in the literature.[47] TEC 10 glass was used for the photoanode, and TEC 7 glass was used for the counter electrode (Hartford Glass). The photoanode consists of a 10 μm mesoporous TiO_2 active layer (particle size, 20 nm, Greatcell Solar, 18NR-T) and a 5.0 μm TiO_2 scattering layer (particle size, 100 nm, Solaronix R/SP). The working photoanode was prepared by immersing the TiO_2 film into a dye solution for 16 h. The dye dipping solution was prepared by using 0.3 mM dye in an ethanol: THF (4:1) solution with CDCA (6 mM). The molar ratio of dye/CDCA was 1:20 in all devices. Devices were tested under two iodide/triiodide (I^-/I_3^-)-based electrolytes named E1I and E2I, prepared as follows: E1I electrolyte: 1.0 M DMII (1,3-dimethylimidazolium iodide), 0.03 M I_2, 0.1 M GuNCS (guanidinium thiocyanate), 0.05 M LiI, and 0.5 M 4-*tert*-butylpyridine (TBP) in acetonitrile/valeronitrile (85:15, v/v). E2I electrolyte is the same as E1I, with the exception of a higher LiI loading (1.0 M).

Device Characterization Information. Current−voltage curves were generated utilizing masked solar cells with a circular active area of 0.15 cm^2. Photovoltaic characterization, including electrochemical impedance spectroscopy (EIS), small modulation photovoltage transient measurements (SMPVT), charge extraction under open-circuit conditions (Q_{oc}) as a function of light intensity, and incident photon-to-current conversion efficiency (IPCE) experiments, were measured, as described in the literature.[48]

ZrO$_2$ and TiO$_2$ Film Formation and Characterization. Photoanodes were prepared as described in literature, with some minor changes in the thickness of the TiO_2 films on the FTO (fluorine-doped tin oxide) TEC 10 glass (Hartford glass).[47] For emission studies, the photoanodes were printed with 2.7 μm mesoporous TiO_2 active layer (particle size, 20 nm, Greatcell Solar, 18NR-T) with no scattering layer. To sensitize the films of the dyes onto the TiO_2 surface, TiO_2 films were immersed into a dye dipping solution for 16 h. The dye dipping solution was prepared by using 0.3 mM dye in an ethanol/THF (4:1) solution with 6 mM chenodeoxycholic acid (CDCA, Chem-Impex International). A similar procedure was done for ZrO_2 surface emission studies, where 2.7 μm ZrO_2 active layer (Zr-nanoxide ZR/SP, Solaronix) was printed on FTO glass (TEC 10, Hartford Glass). For sensitizing dyes onto the ZrO_2 surface, ZrO_2 films were immersed into a dye dipping solution for 16 h. Emission spectra were measured with a Horiba FluoroMax SpectroFluorimeter. The devices were positioned at a 45° angle relative to the light source and

detector, and multiple scans were taken with each film with slight variation in angles to find the maximum emission response. Absorption spectra of dyes on TiO₂ follow the same procedure as described above in the film emission studies. For films without CDCA, the dye dipping solution was made by removing CDCA from the dye dipping solution, and only the dye (0.3 mM) was dipped for 16 h in an ethanol/THF (4:1) solution. The film absorption was measured with an AvaSpec-ULS2048-USB2-50 Spectrometer (Pine Research part RRAVSP3), and the light source was a UV/Vis/NIR Light Source (Pine Research part RRAVSP). These two systems were used in conjunction with the AvaSoft8 software program.

■ RESULTS AND DISCUSSION

Initially, several dual donor, cross-conjugated structures were computationally analyzed with varied atoms fusing two triarylamine benzene rings to aid in selecting a desirable target (Figure S1). Although the intriguing properties of the carbon-fused donors (Figures S2 and S3) were predicted, this design proved synthetically challenging despite attempting multiple routes. However, the silicon-fused system was accessible synthetically through a straightforward route (Scheme 1). The synthesis of QL17 begins with a Horner–Wadsworth–Emmons reaction of ketone 1 and phosphonate ester 2 to give alkene 3 in 86% yield. A microwave-assisted Buchwald coupling is then utilized to react aryl dichloride 3 and amine 4 to yield double donor 5 in 67% yield. A Vilsmeier–Haack formylation of 5 gives aldehyde 6 in 53% yield. The aldehyde 6 undergoes a Knoevenagel condensation to give the final product QL17 in 64% yield. For QL18, the synthesis begins with thiophene intermediate 5, which undergoes lithiation followed by a stannylation to yield product 7 in quantitative yield. A Stille coupling between 7 and bromide 8 (previously reported)[34] gives aldehyde 9 in 61% yield. A Knoevenagel condensation of aldehyde 9 quantitatively yields the final product, QL18.

The dyes were characterized optically and electrochemically (Table 1). QL18 is observed to absorb further into the NIR

Table 1. Optical and Electrochemical Properties of QL17 and QL18 in DCM

dye	λ_{max} (nm)	ε (M^{-1} cm^{-1})	λ_{onset} (nm)[a]	$E_{(S^+/S)}$ (V vs NHE)	$E_{(S^+/S^*)}$ (V vs NHE)[b]	E_g^{opt} (eV)[c]
QL17	520	18 000	648	0.86[d]	−1.05	1.91
QL18	653	66 700	784	0.78	−0.80	1.58
D35[e]	500	31 000	570	1.04	−1.14	2.18
C236/DF15[f]	530	35 000	650	0.94	−0.97	1.91

[a]The absorption onset (λ_{onset}) values were taken by drawing a line of best fit corresponding to the lowest energy transition in the absorption spectrum and extrapolating it to the x-intercept of the graph. [b]$E_{(S^+/S^*)}$ was calculated using the equation $E_{(S^+/S^*)} = E_{(S^+/S)} - E_g^{opt}$. [c]$E_g^{opt}$ was determined by the equation $E_g^{opt} = 1240$ nm × eV/λ_{onset}. [d]Average includes an estimated shoulder value. [e]D35 data was previously reported.[49] [f]C236/DF15 data was previously reported.[50,51]

than QL17, with an absorption onset (λ_{onset}) at about 780 nm, almost 140 nm past the λ_{onset} of QL17 (Table 1 and Figure 3). This red shift is attributed in part to the greater conjugation length of QL18. The molar absorptivity (ε) of QL18 at the absorption maxima (λ_{max}, 66 700 M^{-1} cm^{-1} at 653 nm) is significantly higher than QL17 (18 000 M^{-1} cm^{-1} at 520 nm), which is attributed to the addition of the CPDT and

thienothiophene building blocks. QL18 is observed to have two major transitions, one of lower energy at 653 nm and another at higher energy but lower intensity at 414 nm. The origin of the higher energy transition was studied further computationally (vide infra). Comparison of QL17 to C236/DF15 allows for direct analysis of the effect of an added triarylamine group in a cross-conjugated design (Figure 2). Incorporating the fused donor showed little difference via absorption spectroscopy. Both dyes feature similar onset wavelengths (λ_{onset}, ~650 nm) and λ_{max} (~525 nm) values. However, a broadening of the absorption curve is observed with QL17 in comparing the two dyes. A 33 nm increase is observed with QL17 when the full width at half-maximum of the two dyes are compared.

Gas-phase properties of QL17 and QL18 were studied computationally at the B3LYP/6-311G(d,p) level of theory in isolation (Table 2).[42,46] The computationally predicted vertical transition values are slightly red-shifted in comparison to experimental values for both dyes (Table 2 and Figure 3) by 0.54 and 0.52 eV. Computations show five different orbitals play significant roles in the various transitions of the dyes in the visible spectral region (Figures 4 and S4). The HOMO − 1 resides on the amine group perpendicular to the longest linear conjugated path of QL17. However, in QL18, the HOMO − 1 is diffused across both amines. In both dyes, the HOMO predominantly resides on one amine, while the LUMO resides on the π-bridge and CAA with some overlap in between the two orbital sets. The HOMO and LUMO are the primary orbitals (99% contribution) involved in the S₀ to S₁ transition for QL18. However, the S₀ to S₁ transition is primarily HOMO − 1 to LUMO for QL17 (94% contribution). This suggests ICT is taking place with both of the dyes. The LUMO + 1 of QL17 is very similar in position to the LUMO. The LUMO + 1 of QL18 has less orbital presence on the CAA as compared to its LUMO. The HOMO − 2 of both dyes shows the orbital is present primarily on the π-bridge. For QL18, computation predicts a transition at 454 nm, which likely correlates to the high energy transition observed in the UV−Vis spectrum at ~413 nm. This feature is attributed to the HOMO − 2 to LUMO + 1 transition, as suggested by the computational data. Interestingly, there is only a ~0.02 and ~0.14 eV difference in the HOMO − 1 and HOMO energies for QL17 and QL18, respectively. This indicates both amines have electrons of similar donation strength and are nearly degenerate.

The electrochemical properties of both dyes were analyzed via cyclic voltammetry in dichloromethane. The ground-state oxidation potentials ($E_{(S^+/S)}$) for QL17 and QL18 are 0.86 and 0.78 V vs normal hydrogen electrode (NHE), respectively (Figure 5 and Table 1). In comparing the ground-state oxidation potentials of the two dyes, it can be seen that QL18 is more easily oxidized, which is likely due to the electron-rich nature of CPDT. QL17 and C236/DF15 differ in structure by only the added fused amine donor on QL17. This addition leads to a 80 mV shift in the ground-state oxidation potential to more negative values on the NHE scale. This indicates that cross-conjugation does have an appreciable effect on the electron density provided by the donor. Similarly, the electron-rich substituents on QL18 allow it to be more easily oxidized in comparison to benchmarks D35 and C236/DF15. QL17 and C236/DF15 have near identical excited-state oxidation potentials ($E_{(S^+/S^*)}$). However, QL18 has a much more positive excited-state oxidation potential (−0.80 V vs −1.05 V for QL17), which is likely due to the addition of the auxiliary
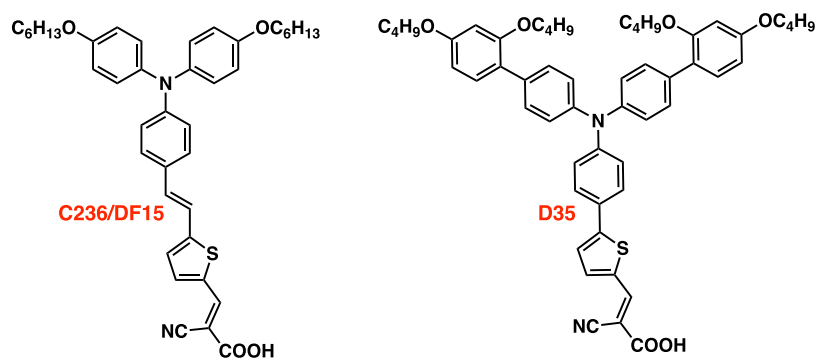
Figure 2. Structures of **C236/DF15** and **D35**.

Table 2. Select TD-DFT Data for QL17 and QL18

dye	state	orbitals	contribution (%)[a]	vert. trans. (nm | eV)	oscillator strength
QL17	S0 → S1	HOMO − 1 → LUMO	94	673 | 1.84	0.1134
		HOMO → LUMO	6		
	S0 → S2	HOMO → LUMO	94	638 | 1.94	0.4810
	S0 → S3	HOMO − 2 → LUMO	93	437 | 2.84	0.5694
QL18	S0 → S1	HOMO → LUMO	99	898 | 1.38	0.5514
	S0 → S3	HOMO − 2 → LUMO	96	664 | 1.88	0.9513
	S0 → S4	HOMO → LUMO + 1	83	551 | 2.25	0.6536
	S0 → S5	HOMO − 1 → LUMO + 1	89	517 | 2.40	0.1164
	S0 → S7	HOMO − 2 → LUMO + 1	87	454 | 2.73	0.2750

[a]Minor orbital contributions to each state are listed in the Supporting Information. Transitions are only reported for the visible region with oscillator strengths >0.1. Data collected at the B3LYP/6-311G(d,p) level of theory.
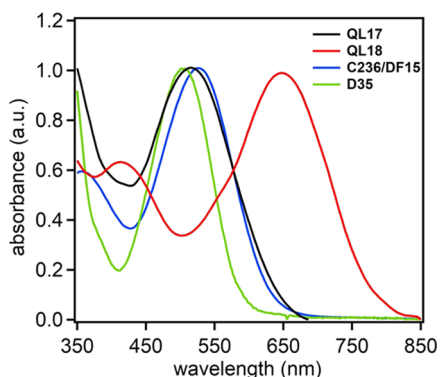

Figure 3. Normalized absorption spectra of **QL17**, **QL18**, **C236/DF15**, and **D35** in DCM.

acceptor thienothiophene being strongly electron-withdrawing. Importantly, solution measurements suggest there is sufficient driving force for rapid electron transfer from the photoexcited dyes into the CB of TiO_2 and electron transfer from the I^-/I_3^- redox shuttle to the ground-state oxidized dyes. This indicates the dyes will be functional photosensitizers in DSC devices.

DSC devices were fabricated with **QL17**, **QL18**, **D35**, and **C236/DF15** in two different (I^-/I_3^-)-based electrolytes, E1I (0.05 M LiI) and E2I (1.0 M LiI). Device performances were investigated using an AM 1.5G solar simulated spectrum at 1 sun intensity as a light source. **QL17** performed better than **QL18** in terms of photocurrent (2.8 mA/cm^2 higher) and photovoltage (~110 mV higher) with the E1I electrolyte. By switching to the E2I electrolyte, a significant photocurrent increase in **QL18** is observed, from 4.7 to 10.8 mA/cm^2, which is attributed to higher concentrations of LiI (Table 3). Higher concentrations of LiI facilitate facile electron transfer by

downward shifting of the CB of the $_2$ film[3,52−55] and improve the injection rate, which enhances the measured photocurrent.[56,57] This suggests the excited-state oxidation potential of **QL18** does not provide a sufficient over potential for facile electron injection into the CB of TiO_2 without the addition of LiI to lower the CB. A similar significant shift in photocurrent was observed for **D35** and **C236/DF15** when changing the electrolyte from E1I to E2I, where the current for **D35** increases to 13.5 from 12.6 mA/cm^2. For **C236/DF15**, values increased to 14.0 from 10.4 mA/cm^2. In the case of **QL17**, only a slight increase in photocurrent (0.5 mA/cm^2) is observed when switching from E1I to the E2I electrolyte. Despite the lower photocurrents observed with **QL17** and **QL18** compared to the benchmark materials, a shift in the IPCE spectra onset of **QL18** to lower energies (~900 nm) is observed relative to **D35** and **C236/DF15**, which have IPCE onsets of ~750 and ~775 nm, respectively (Figure 6, bottom). Notably, few organic sensitizers can produce electricity from photons ≥900 nm.[8] However, **QL18** shows a low peak IPCE value (15% with E1I and 30% with E2I), which yields a less-than-optimal photocurrent for a device with an IPCE onset near 900 nm. **QL17** shows a higher peak IPCE than **QL18** at 55% in E2I electrolyte. The increase in the peak IPCE values with **QL17** and **QL18** upon increasing LiI loading is indicative of poor injection efficiency, likely due to aggregation based on the **QL18** IPCE curve shape differing substantially from the solution absorption curve shape. This is further supported by the drastic difference in the absorption spectra of **QL18** on TiO_2 with and without CDCA (Figure S16), suggesting that despite the abundant alkyl chains on the donor, these dyes are still aggregating on the TiO_2 surface. Moreover, further device studies were carried out at varying CDCA concentrations and showed increased performances for both **QL17** and **QL18** as
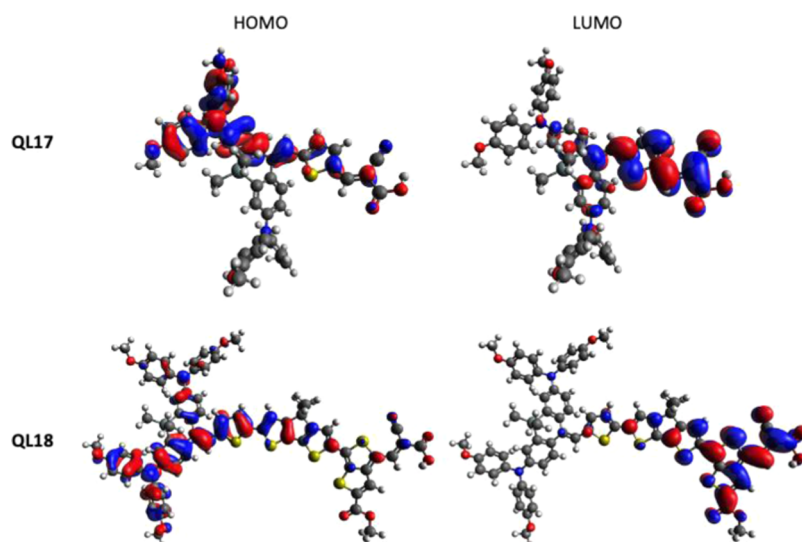
Figure 4. HOMO and LUMO orbitals obtained at the B3LYP/6-311G(d,p) level of theory.
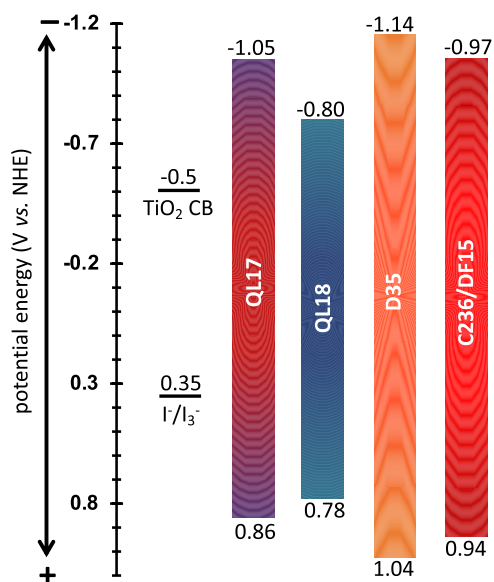

Figure 5. Energy level diagram for **QL17** and **QL18**.

CDCA increased (Tables S5 and S6). Electron injection efficiencies were probed via steady-state emission curve areas of the dyes on TiO_2 and ZrO_2, and estimated injection efficiency values ranged from 58 to 97% and followed the trend

QL18 (58%) < **QL17** (62%) < **C236/DF15** (91%) < **D35** (97%) (Table S4 and Figures S9–S12).

In terms of photovoltage, **QL17** has a higher photovoltage (687 mV) compared to literature dye **C236/DF15** (676 mV). This suggests better surface protection from the cross-conjugated donor, which is much more heavily alkylated. Increasing the number of alkyl chains often leads to increased photovoltages by reducing recombination rates.[26,58] The power conversion efficiency (PCE) was calculated according to the equation $PCE = \frac{J_{SC} \times FF \times V_{OC}}{I_0}$, where J_{SC} is the short-circuit current density, FF is the fill factor, V_{OC} is the open-circuit voltage, and I_0 is the intensity of incident light set to 1 sun for these studies unless otherwise noted (Table 3). There is a significant increase in PCE for **QL18** when replacing E1I with E2I as PCE increased from 1.8 to 3.5% due to a significant increase in photocurrent in the E2I electrolyte. PCE is similar for **QL17** and **QL18** in the E2I electrolyte.

Apart from **QL18**, all of the dyes performed better in terms of PCE with low LiI concentrations in the E1I electrolyte. Further device characterization studies were taken using E1I as the electrolyte for all of the dyes, in addition to analysis of **QL18** with the E2I electrolyte. Electrochemical impedance spectroscopy (EIS) experiments were conducted at open-circuit potential bias to probe electron-transfer resistances and electron lifetimes. These experiments were conducted under an

Table 3. Photovoltaic Performance Data for the DSC Devices[a]

dye	electrolyte	PCE (%)	J_{SC} (mA/cm²)	integrated J_{SC}	V_{OC} (mV)	FF (%)	Γ[b] (mol/cm²)
QL17	E1	4.3 ± 0.1	7.5 ± 0.4	6.57	687 ± 10	71 ± 1	1.33×10^{-8}
	E2	3.2 ± 0.0	8.0 ± 0.1	8.18	591 ± 08	69 ± 2	
QL18	E1	1.8 ± 0.1	4.7 ± 0.2	5.32	573 ± 07	71 ± 1	9.65×10^{-9}
	E2	3.5 ± 0.3	10.8 ± 0.9	11.5	552 ± 22	74 ± 3	
D35	E1	6.4 ± 0.1	12.6 ± 0.2	12.7	734 ± 08	70 ± 1	2.62×10^{-8}
	E2	4.5 ± 0.1	13.5 ± 0.7	12.8	611 ± 12	55 ± 1	
C236/DF15	E1	4.9 ± 0.1	10.4 ± 0.4	10.5	676 ± 07	71 ± 1	1.94×10^{-8}
	E2	4.6 ± 0.3	14.0 ± 0.1	13.4	564 ± 09	58 ± 3	

[a]Values are the average of two DSC devices. [b]Dye loading for the sensitized films calculated using the equation $\Gamma = [A(\lambda)/\varepsilon(\lambda)]/1000$, where Γ is the dye loading in mol/cm², $A(\lambda)$ is the measured absorption of the film at the maximum wavelength for the respective dye, and $\varepsilon(\lambda)$ is the molar absorptivity of the respective dye.[59]
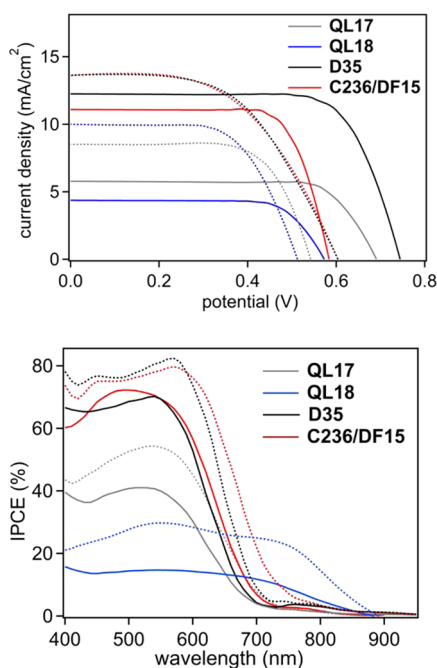
Figure 6. Current density (J) versus the applied voltage (V) curves (top) and IPCE curves (bottom) of **QL17**, **QL18**, **D35**, and **C236/DF15**. Solid lines represent devices with electrolyte E1I: 1.0 M DMII (1,3-dimethylimidazolium iodide), 0.03 M I$_2$, 0.1 M GuNCS (guanidinium thiocyanide), 0.05 M LiI, and 0.5 M 4-*tert*-butylpyridine (TBP) in acetonitrile/valeronitrile (85:15, v/v) solvent. Dashed lines represent devices with electrolyte E2I, which has the same components as E1, except with a higher LiI loading (1.0 M).

AM 1.5G solar simulated spectrum at 1 sun intensity as a light source. Although EIS can be conducted under dark conditions, these conditions generate an environment that is not usually representative of the typical working cell under illuminated conditions.[2] Specifically, back electron transfer from TiO$_2$ to the oxidized dye becomes an excluded process, and increased current flow can be observed. While a dark EIS measurement is able to directly probe charge recombination rates between TiO$_2$ and the RS, the results are reflective of an idealistic cell without the competing factor of back electron transfer to the oxidized dye as well as decreased electrode heat; thus, EIS measurements were conducted under illumination.[2] The data was fitted using a template circuit (Figure 7) to generate the Nyquist and Bode plots (Figures 7 and S7). The Nyquist plot consists of two semicircles, the smaller of which represents the resistance of electron transfer at the electrolyte−counter electrode interface (R_{CE}) (Figure 7 and Table 4). The larger semicircle represents the resistance to recombination of electrons from the TiO$_2$ CB to the electrolyte (R_{rec}). The Nyquist plot shows that R_{rec} is lowest for the **C236/DF15** devices (16.54 Ω) and largest for **QL18** (47.58 Ω). Ideally, the R_{rec} term should be as large as possible to slow nonproductive electron-transfer events. **QL17** has a smaller R_{rec} (25.03 Ω) as compared to **QL18** (47.58 Ω). R_{rec} exhibits the following trend: **C236/DF15** < **D35** < **QL17** < **QL18** (Table 4). This indicates that detrimental recombination processes are more likely with **D35** and **C236/DF15**, and less likely with **QL17** and **QL18**. The larger R_{rec} values observed for **QL17** and **QL18** is attributed to an increase in the number of alkyl chains on the bulky dibenzosilin donor group, which insulates the TiO$_2$ surface from the electrolyte.[26,58] In comparing the E1I vs
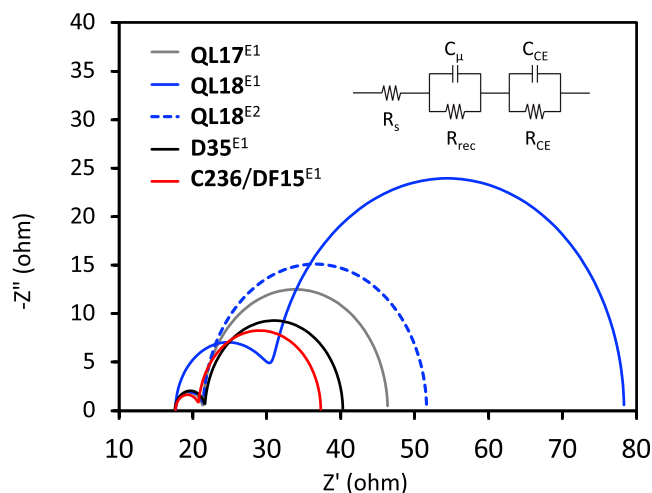

Figure 7. Nyquist plot of **QL18**, **QL17**, **D35**, and **C236/DF15**. Superscripts E1 and E2 are for iodine-based electrolytes, E1I and E2I.

Table 4. Summary of EIS Data of the DSC Device[a]

device	R_{CE} (Ω)	R_{rec} (Ω)	C_μ (mF)	C_{CE} (F)	η_{cc} (%)
QL17[E1]	3.78	25.03	1.28	7.59×10^{-6}	87
QL18[E1]	13.10	47.58	0.43	1.57×10^{-5}	78
QL18[E2]	3.79	30.22	1.05	1.49×10^{-5}	89
D35[E1]	4.07	18.61	1.03	7.67×10^{-5}	82
C236/DF15[E1]	3.13	16.54	0.67	1.25×10^{-5}	84

[a]R_{rec} is the recombination resistance of electrons in TiO$_2$ across the TiO$_2$−dye interface to an oxidized redox shuttle, R_{CE} is the electron-transfer resistance at the counter electrode to an oxidized redox shuttle, C_μ is the chemical capacitance for charge accumulation in TiO$_2$, and C_{CE} is the capacitance at the electrolyte−counter electrode interface. $\eta_{cc} = 1/(1 + (R_{CE}/R_{rec}))$, where η_{cc} is the charge collection efficiency.

E2I data for **QL18**, charge recombination is observed to be more favorable with E2I (Table 4). Despite a higher observed R_{rec} for **QL18**, the V_{OC} for **QL18**-based DSC devices is lower than that of **QL17**. It is noteworthy that a higher charge collection efficiency (discussion below) is found with **QL17** due to a lower R_{CE} value, which correlates to the higher V_{OC} observed for the **QL17**-based device. While the origin for the higher R_{CE} value is not apparent from these studies, a plausible explanation for this could be due to dye aggregation not allowing efficient transport of charge and leading to depletion of oxidizing electrolyte at the counter electrode during steady-state illumination, as has been previously noted.[60] **D35** and **C236/DF15** both exhibit higher dye loadings than the **QL** dyes (Table 3). The **QL** dyes both showed greater R_{rec} (Table 4), which suggests that the surface protection that is provided by the two dyes having donors with a large number of alkyl chains is substantial. However, the observed aggregation can lead to reduced charge injection efficiency (see studies below) and increased back electron transfer to the dye, which lowers photovoltages and photocurrents. Notably, all of the devices have good charge collection efficiency (η_{cc}) values that range from 78 to 89% according to the equation $\eta_{cc} = 1/(1 + (R_{CE}/R_{rec}))$ due to the low resistance of the electron transfer at the platinum counter electrode (Table 4). In the E1I conditions, **QL18** is observed to have the lowest charge collection efficiency (78%). An increase in η_{cc} is observed from the E2I conditions (89%), which is likely contributing to higher J_{SC}

values and, subsequently, IPCE values as well (Table 3 and Figure 6).

To probe shifts in the CB of TiO_2, charge extraction measurements were carried out under open-circuit conditions at varied light intensities. The relative CB shift can be estimated via the charge extraction measurements by comparing the horizontal displacement of the curves at a given capacitance (Figure 8).[61,62] In comparing **QL18** in E1I
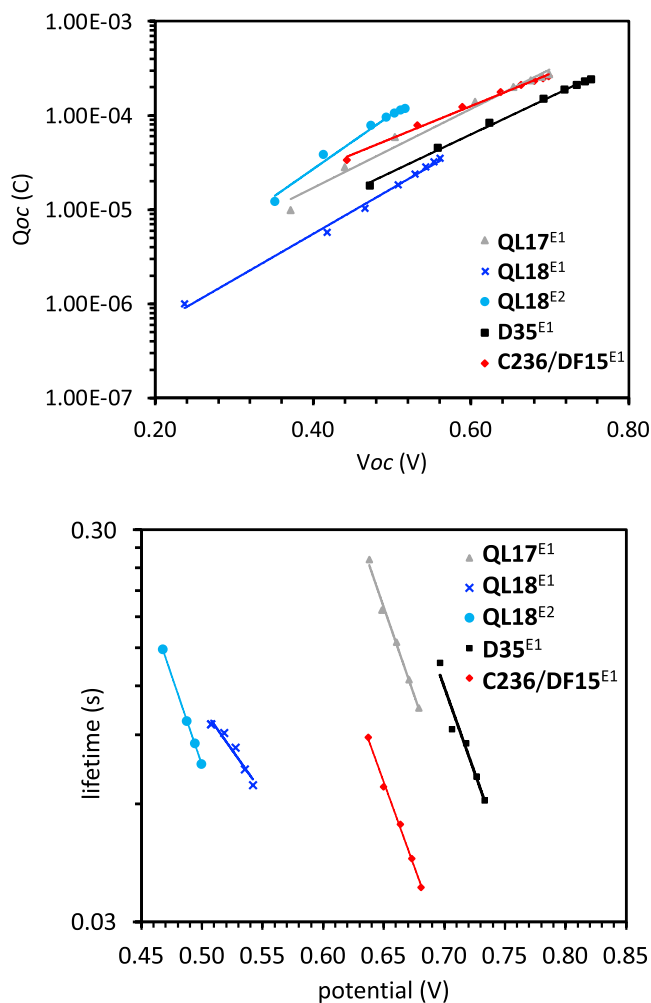

Figure 8. Charge extraction (top) and SMPVT (bottom) of **QL17**, **QL18**, **D35**, and **C236/DF15**.

vs E2I conditions, it is observed that the conduction band of TiO_2 is lowered by ~150 mV in conditions with higher lithium loading. Higher lithium loadings usually result in lower V_{OC} values, and in comparing the E1I and E2I conditions in **QL18**-based DSC devices, the V_{OC} in devices using the E2I electrolyte is 21 mV lower than that of E1I. Thus, the photovoltage loss from the downward shift of the CB due to increased Li^+ concentration is offset by a higher η_{cc} with E2I, which increases the measured photovoltage by reducing recombination losses. Additionally, in comparing **QL17** and **QL18**, it is seen that **QL17** has higher photovoltage in both electrolytes. The photovoltage loss observed in **QL18** can be attributed to aggregation, given the significant absorption curve shape change in films made with and without CDCA in comparison to **QL17** (Figures S15 and S16). Electron injection efficiency studies were conducted by comparing the

emission of the dyes on TiO_2 and ZrO_2 (an insulator). The emission intensity decreases as electrons are injected into TiO_2 relative to ZrO_2, which does not allow interfacial electron transfer. In this case, steady-state emission curve areas were used to estimate injection efficiency, where the film's emission was measured by placing the film at an angle to give the highest emission observable (at or near 45° in the fluorometer). These studies reveal **QL17** and **QL18** have the lowest injection efficiencies of 62 and 58%, respectively, in comparison to much higher efficiencies for **D35** (97%) and **C236/DF15** (91%) (Table S4). Thus, it is likely that lower electron injection efficiencies due to surface aggregation are contributing to photovoltage losses for both **QL** dyes by reducing the number of electrons in TiO_2 and enabling back electron transfer to lower energy electron accepting aggregates. Furthermore, there is about a 50 mV CB shift due to dye structure when comparing **QL17** and **D35** with a lower CB energy for **QL17** devices. Small modulated photovoltage transient (SMPVT) measurements were undertaken to better understand the charge separation lifetime (a measure of the recombination rate of electrons in TiO_2 with the electrolyte) as a function of applied light intensity (Figure 8).[63] The electron lifetime in TiO_2 of the devices follows the order **D35** > **QL17** > **C236/DF15** > **QL18**. **QL17** has about 2 orders of magnitude longer electron lifetime than **QL18**, which could be due to the orientation of the dye on TiO_2, where a donor closer to the TiO_2 surface results in faster recombination (Figure S8).[3] Interestingly, **D35** shows a modestly longer electron lifetime than **QL17** (~0.01 s longer), which differs from the EIS measurements where R_{rec} is greater for **QL17**. The origin of this subtle difference is not apparent from these studies, although it is important to note that the two measurements function differently in that voltages are directly applied in EIS and photogenerated in SMPVT, leading to potential differences in the measurements.

◼ CONCLUSIONS

Herein, two novel silicon-fused double donor cross-conjugated dyes are reported. Computational data reveals the participation of both donors in ICT. Computational data also shows that all of the dyes have well-positioned orbitals for facile photo-induced interfacial charge separation on TiO_2. The two silicon-based dyes have solution absorption onsets of about 780 and 640 nm for **QL18** and **QL17**, respectively. In conjunction with solution electrochemical data via cyclic voltammetry, excited-state oxidation potentials of −1.05 and −0.80 V vs NHE are observed for **QL17** and **QL18**, respectively. These solution measured values are sufficiently high for facile electron transfer to TiO_2, which is often challenging for dyes absorbing photons in the near-infrared region. DSC devices were studied through current−voltage curves, IPCEs, SMPVT experiments, electrochemical impedance spectroscopy, and charge extraction measurements. Current−voltage curves show that the two dyes have comparable V_{OC} values of about 550 mV in E2I conditions. **QL18** is able to generate more photocurrent than **QL17** under E2I conditions by almost 3 mA/cm². IPCE curves reveal a near 900 nm onset for **QL18**, which is exceptional for an organic chromophore. SMPVT reveals lifetimes of multiple orders of magnitude greater for **QL17** in comparing the two novel dyes. EIS data reveal greater resistance to charge recombination for **QL18** in E1I conditions. **QL18** and **QL17** both feature 6 alkyl chains on the dibenzosilin donor, which prevents detrimental recombination events and provides high

recombination resistance. Notably, better recombination resistance is observed with the **QL** dyes than with **D35**, as seen by EIS. **D35** is a well-known dye with outstanding surface protection that, in part, allowed for the use of transition-metal-based redox shuttles where exceptional recombination resistances are needed. Dyes with better recombination resistance than **D35** are rare. Future studies with dibenzosilin-based dyes would involve improving the peak IPCE values through dye designs that allow for higher $E_{(S+/S*)}$ and reduced dye conformations in order to facilitate better injection, which would help improve the photovoltages and photocurrents generated in DSC devices.

ASSOCIATED CONTENT

Supporting Information

The Supporting Information is available free of charge at https://pubs.acs.org/doi/10.1021/acsomega.3c02571.

Computational data, electrochemical data, device data, and NMR data (PDF)

AUTHOR INFORMATION

Corresponding Author

Jared H. Delcamp − *Department of Chemistry and Biochemistry, University of Mississippi, University, Mississippi 38677, United States; Materials and Manufacturing Directorate, Air Force Research Laboratory, Wright-Patterson AFB, Ohio 45433, United States; UES Inc., Dayton, Ohio 45432, United States;* orcid.org/0000-0001-5313-4078; Email: jared.delcamp.ctr@us.af.mil

Authors

Qing Yun Li − *Department of Chemistry and Biochemistry, University of Mississippi, University, Mississippi 38677, United States;* orcid.org/0000-0001-6723-5195

Ravinder Kaur − *Department of Chemistry and Biochemistry, University of Mississippi, University, Mississippi 38677, United States;* orcid.org/0000-0002-9394-4451

William E. Meador − *Department of Chemistry and Biochemistry, University of Mississippi, University, Mississippi 38677, United States;* orcid.org/0000-0002-9869-026X

Juganta K. Roy − *Interdisciplinary Center for Nanotoxicity, Department of Chemistry, Physics and Atmospheric Sciences, Jackson State University, Jackson, Mississippi 39217, United States;* orcid.org/0000-0002-3646-5593

Jerzy Leszczynski − *Interdisciplinary Center for Nanotoxicity, Department of Chemistry, Physics and Atmospheric Sciences, Jackson State University, Jackson, Mississippi 39217, United States;* orcid.org/0000-0001-5290-6136

Complete contact information is available at:
https://pubs.acs.org/10.1021/acsomega.3c02571

Author Contributions

[1]Q.Y.L. and R.K. contributed equally.

Notes

The authors declare no competing financial interest.

ACKNOWLEDGMENTS

REFERENCES

(1) Gong, J.; Li, C.; Wasielewski, M. R. Advances in Solar Energy Conversion. *Chem. Soc. Rev.* **2019**, *48*, 1862−1864.

(2) Muñoz-García, A. B.; Benesperi, I.; Boschloo, G.; Concepcion, J. J.; Delcamp, J. H.; Gibson, E. A.; Meyer, G. J.; Pavone, M.; Pettersson, H.; Hagfeldt, A.; Freitag, M. Dye-Sensitized Solar Cells Strike Back. *Chem. Soc. Rev.* **2021**, *50*, 12450−12550.

(3) Hagfeldt, A.; Boschloo, G.; Sun, L.; Kloo, L.; Pettersson, H. Dye-Sensitized Solar Cells. *Chem. Rev.* **2010**, *110*, 6595−6663.

(4) O'Regan, B.; Grätzel, M. A Low-Cost, High-Efficiency Solar Cell Based on Dye-Sensitized Colloidal TiO2 Films. *Nature* **1991**, *353*, 737−740.

(5) Venkatesan, S.; Hsu, T.-H.; Teng, H.; Lee, Y.-L. Dye-Sensitized Solar Cells with Efficiency over 36% under Ambient Light Achieved by Cosensitized Tandem Structure. *Sol. RRL* **2023**, *7*, No. 2300220.

(6) Michaels, H.; Rinderle, M.; Freitag, R.; Benesperi, I.; Edvinsson, T.; Socher, R.; Gagliardi, A.; Freitag, M. Dye-Sensitized Solar Cells under Ambient Light Powering Machine Learning: Towards Autonomous Smart Sensors for the Internet of Things. *Chem. Sci.* **2020**, *11*, 2895−2906.

(7) Michaels, H.; Benesperi, I.; Freitag, M. Challenges and Prospects of Ambient Hybrid Solar Cell Applications. *Chem. Sci.* **2021**, *12*, 5002−5015.

(8) Brogdon, P.; Cheema, H.; Delcamp, J. H. Near-Infrared-Absorbing Metal-Free Organic, Porphyrin, and Phthalocyanine Sensitizers for Panchromatic Dye-Sensitized Solar Cells. *ChemSusChem* **2018**, *11*, 86−103.

(9) Ji, J.-M.; Zhou, H.; Kim, H. K. Rational Design Criteria for D−π−A Structured Organic and Porphyrin Sensitizers for Highly Efficient Dye-Sensitized Solar Cells. *J. Mater. Chem. A* **2018**, *6*, 14518−14545.

(10) Luo, J.; Xie, Z.; Zou, J.; Wu, X.; Gong, X.; Li, C.; Xie, Y. Efficient Dye-Sensitized Solar Cells Based on Concerted Companion Dyes: Systematic Optimization of Thiophene Units in the Organic Dye Components. *Chin. Chem. Lett.* **2022**, *33*, 4313−4316.

(11) Wang, X.; Wang, Y.; Zou, J.; Luo, J.; Li, C.; Xie, Y. Efficient Solar Cells Sensitized by Organic Concerted Companion Dyes Suitable for Indoor Lamps. *ChemSusChem* **2022**, *15*, No. e202201116.

(12) Zou, J.; Wang, Y.; Baryshnikov, G.; Luo, J.; Wang, X.; Ågren, H.; Li, C.; Xie, Y. Efficient Dye-Sensitized Solar Cells Based on a New Class of Doubly Concerted Companion Dyes. *ACS Appl. Mater. Interfaces* **2022**, *14*, 33274−33284.

(13) Chou, C.-C.; Wu, K.-L.; Chi, Y.; Hu, W.-P.; Yu, S. J.; Lee, G.-H.; Lin, C.-L.; Chou, P.-T. Ruthenium(II) Sensitizers with Heteroleptic Tridentate Chelates for Dye-Sensitized Solar Cells. *Angew. Chem., Int. Ed.* **2011**, *50*, 2054−2058.

(14) Numata, Y.; Singh, S. P.; Islam, A.; Iwamura, M.; Imai, A.; Nozaki, K.; Han, L. Enhanced Light-Harvesting Capability of a Panchromatic Ru(II) Sensitizer Based on π-Extended Terpyridine with a 4-Methylstylryl Group for Dye-Sensitized Solar Cells. *Adv. Funct. Mater.* **2013**, *23*, 1817−1823.

(15) Nazeeruddin, M. K.; Péchy, P.; Renouard, T.; Zakeeruddin, S. M.; Humphry-Baker, R.; Comte, P.; Liska, P.; Cevey, L.; Costa, E.; Shklover, V.; Spiccia, L.; Deacon, G. B.; Bignozzi, C. A.; Grätzel, M. Engineering of Efficient Panchromatic Sensitizers for Nanocrystalline TiO2-Based Solar Cells. *J. Am. Chem. Soc.* **2001**, *123*, 1613−1624.

(16) Abbotto, A.; Sauvage, F.; Barolo, C.; Angelis, F. D.; Fantacci, S.; Graetzel, M.; Manfredi, N.; Marinzi, C.; Nazeeruddin, M. K. Panchromatic Ruthenium Sensitizer Based on Electron-Rich Heteroarylvinylene π-Conjugated Quaterpyridine for Dye-Sensitized Solar Cells. *Dalton Trans.* **2011**, *40*, 234−242.

(17) Chen, C.-Y.; Feng, Y.-M.; Wu, T.-Y.; Liu, Y.-C.; Chen, S.-Y.; Lin, T.-Y.; Tsai, H.-H. G.; Wu, C.-G. Terpyridyl Ruthenium

Complexes Functionalized with Conjugated Heterocycles for Panchromatic Dye-Sensitized Solar Cells. *ACS Appl. Energy Mater.* **2021**, *4*, 13461−13470.

(18) Kandregula, G. R.; Mandal, S.; Ramanujam, K. Molecular Engineering of Near-Infrared Active Boron Dipyrromethene Moiety with Various Donors and Acceptors for Tuning the Absorption Behavior and Electron Injection of the Resultant Dyes. *J. Photochem. Photobiol. A* **2021**, *410*, No. 113161.

(19) Punitharasu, V.; Kavungathodi, M. F. M.; Singh, A. K.; Nithyanandhan, J. π-Extended Cis - Configured Unsymmetrical Squaraine Dyes for Dye-Sensitized Solar Cells: Panchromatic Response. *ACS Appl. Energy Mater.* **2019**, *2*, 8464−8472.

(20) Mathew, S.; Yella, A.; Gao, P.; Humphry-Baker, R.; Curchod, B. F. E.; Ashari-Astani, N.; Tavernelli, I.; Rothlisberger, U.; Nazeeruddin, M. K.; Grätzel, M. Dye-Sensitized Solar Cells with 13% Efficiency Achieved through the Molecular Engineering of Porphyrin Sensitizers. *Nat. Chem.* **2014**, *6*, 242−247.

(21) Hardin, B. E.; Snaith, H. J.; McGehee, M. D. The Renaissance of Dye-Sensitized Solar Cells. *Nat. Photonics* **2012**, *6*, 162−169.

(22) Kang, S. H.; Jeong, M. J.; Eom, Y. K.; Choi, I. T.; Kwon, S. M.; Yoo, Y.; Kim, J.; Kwon, J.; Park, J. H.; Kim, H. K. Porphyrin Sensitizers with Donor Structural Engineering for Superior Performance Dye-Sensitized Solar Cells and Tandem Solar Cells for Water Splitting Applications. *Adv. Energy Mater.* **2017**, *7*, No. 1602117.

(23) Eom, Y. K.; Kang, S. H.; Choi, I. T.; Yoo, Y.; Kim, J.; Kim, H. K. Significant Light Absorption Enhancement by a Single Heterocyclic Unit Change in the π-Bridge Moiety from Thieno[3,2-b]Benzothiophene to Thieno[3,2-b]Indole for High Performance Dye-Sensitized and Tandem Solar Cells. *J. Mater. Chem. A* **2017**, *5*, 2297−2308.

(24) Tsao, H. N.; Yi, C.; Moehl, T.; Yum, J.-H.; Zakeeruddin, S. M.; Nazeeruddin, M. K.; Grätzel, M. Cyclopentadithiophene Bridged Donor−Acceptor Dyes Achieve High Power Conversion Efficiencies in Dye-Sensitized Solar Cells Based on the Tris-Cobalt Bipyridine Redox Couple. *ChemSusChem* **2011**, *4*, 591−594.

(25) Zhang, D.; Stojanovic, M.; Ren, Y.; Cao, Y.; Eickemeyer, F. T.; Socie, E.; Vlachopoulos, N.; Moser, J.-E.; Zakeeruddin, S. M.; Hagfeldt, A.; Grätzel, M. A Molecular Photosensitizer Achieves a *V*oc of 1.24 V Enabling Highly Efficient and Stable Dye-Sensitized Solar Cells with Copper(II/I)-Based Electrolyte. *Nat. Commun.* **2021**, *12*, No. 1777.

(26) Baumann, A.; Curiac, C.; Delcamp, J. H. The Hagfeldt Donor and Use of Next-Generation Bulky Donor Designs in Dye-Sensitized Solar Cells. *ChemSusChem* **2020**, *13*, 2503−2512.

(27) Hagberg, D. P.; Yum, J.-H.; Lee, H.; De Angelis, F.; Marinado, T.; Karlsson, K. M.; Humphry-Baker, R.; Sun, L.; Hagfeldt, A.; Grätzel, M.; Nazeeruddin, M. K. Molecular Engineering of Organic Sensitizers for Dye-Sensitized Solar Cell Applications. *J. Am. Chem. Soc.* **2008**, *130*, 6259−6266.

(28) Capodilupo, A. L.; De Marco, L.; Fabiano, E.; Giannuzzi, R.; Scrascia, A.; Carlucci, C.; Corrente, G. A.; Cipolla, M. P.; Gigli, G.; Ciccarella, G. New Organic Dyes Based on a Dibenzofulvene Bridge for Highly Efficient Dye-Sensitized Solar Cells. *J. Mater. Chem. A* **2014**, *2*, 14181−14188.

(29) Wielopolski, M.; Marszalek, M.; Brunetti, F. G.; Joly, D.; Calbo, J.; Aragó, J.; Moser, J.-E.; Humphry-Baker, R.; Zakeeruddin, S. M.; Delgado, J. L.; Grätzel, M.; Ortí, E.; Martín, N. Synthesis and Optoelectronic Properties of Chemically Modified Bi-Fluorenylidenes. *J. Mater. Chem. C* **2016**, *4*, 3798−3808.

(30) Zhou, P.; Liang, J.; Lin, B.; An, Z.; Chen, R.; Chen, X.; An, Q.; Chen, P. Effect of the Spatial Configuration of Donors on the Photovoltaic Performance of Double D−π−A Organic Dyes. *ACS Appl. Mater. Interfaces* **2021**, *13*, 40648−40655.

(31) Chen, Y.-H.; Chen, C.-C.; Nguyen, V. S.; Lu, M.-N.; Chen, Y.-D.; Lin, Y.-C.; Wei, T.-C.; Yeh, C.-Y. Modified Hagfeldt Donor for Organic Dyes That Are Compatible with Copper Electrolytes in Efficient Dye-Sensitized Solar Cells. *ACS Appl. Energy Mater.* **2022**, *5*, 13544−13553.

(32) Chen, C.-C.; Chen, Y.-H.; Nguyen, V. S.; Chen, S.-Y.; Tsai, M.-C.; Chen, J.-S.; Lin, S.-Y.; Wei, T.-C.; Yeh, C.-Y. Double Fence Porphyrins Featuring Indacenodithiophene Group as an Effective Donor for High-Efficiency Dye-Sensitized Solar Cells. *Adv. Energy Mater.* **2023**, *13*, No. 2300353.

(33) Liu, J.; Yang, X.; Zhao, J.; Sun, L. Tuning Band Structures of Dyes for Dye-Sensitized Solar Cells: Effect of Different π-Bridges on the Performance of Cells. *RSC Adv.* **2013**, *3*, 15734−15743.

(34) Cheema, H.; Watson, J.; Peddapuram, A.; Delcamp, J. H. A 25 mA cm^{-2} Dye-Sensitized Solar Cell Based on a near-Infrared-Absorbing Organic Dye and Application of the Device in SSM-DSCs. *Chem. Commun.* **2020**, *56*, 1741−1744.

(35) Hu, Y.; Abate, A.; Cao, Y.; Ivaturi, A.; Zakeeruddin, S. M.; Grätzel, M.; Robertson, N. High Absorption Coefficient Cyclopentadithiophene Donor-Free Dyes for Liquid and Solid-State Dye-Sensitized Solar Cells. *J. Phys. Chem. C* **2016**, *120*, 15027−15034.

(36) Brogdon, P.; Giordano, F.; Puneky, G. A.; Dass, A.; Zakeeruddin, S. M.; Nazeeruddin, M. K.; Grätzel, M.; Tschumper, G. S.; Delcamp, J. H. A Computational and Experimental Study of Thieno[3,4-b]Thiophene as a Proaromatic π-Bridge in Dye-Sensitized Solar Cells. *Chem. − Eur. J.* **2016**, *22*, 694−703.

(37) Mátravölgyi, B.; Hergert, T.; Thurner, A.; Varga, B.; Sangiorgi, N.; Bendoni, R.; Zani, L.; Reginato, G.; Calamante, M.; Sinicropi, A.; Sanson, A.; Faigl, F.; Mordini, A. Synthesis and Investigation of Solar-Cell Photosensitizers Having a Fluorazone Backbone. *Eur. J. Org. Chem.* **2017**, *2017*, 1843−1854.

(38) Meador, W. E.; Lin, E. Y.; Lim, I.; Friedman, H. C.; Ndaleh, D.; Shaik, A. K.; Hammer, N. I.; Yang, B.; Caram, J. R.; Sletten, E. M.; Delcamp, J. H. Shortwave Infrared Absorbing and Emitting Silicon-Rosindolizine Fluorophores for in Vivo Fluorescence Imaging, 2023, under review.

(39) Connelly, N. G.; Geiger, W. E. Chemical Redox Agents for Organometallic Chemistry. *Chem. Rev.* **1996**, *96*, 877−910.

(40) Weast, R. C.; Astle, M. J. *CRC Handbook of Chemistry and Physics: A Ready-Reference Book of Chemical and Physical Data*; CRC Press: Boca Raton, FL, 1982.

(41) Frisch, M. J.; Trucks, G. W.; Schlegel, H. B.; Scuseria, G. E.; Robb, M. A.; Cheeseman, J. R.; Scalmani, G.; Barone, V.; Petersson, G. A.; Nakatsuji, H.; Li, X.; Caricato, M.; Marenich, A. V.; Bloino, J.; Janesko, B. G.; Gomperts, R.; Mennucci, B.; Hratchian, H. P.; Ortiz, J. V.; Izmaylov, A. F.; Sonnenberg, J. L.; Williams-Young, D.; Ding, F.; Lipparini, F.; Egidi, F.; Goings, J.; Peng, B.; Petrone, A.; Henderson, T.; Ranasinghe, D.; Zakrzewski, V. G.; Gao, J.; Rega, N.; Zheng, G.; Liang, W.; Hada, M.; Ehara, M.; Toyota, K.; Fukuda, R.; Hasegawa, J.; Ishida, M.; Nakajima, T.; Honda, Y.; Kitao, O.; Nakai, H.; Vreven, T.; Throssell, K.; Montgomery Jr., J. A.; Peralta, J. E.; Ogliaro, F.; Bearpark, M. J.; Heyd, J. J.; Brothers, E. N.; Kudin, K. N.; Staroverov, V. N.; Keith, T. A.; Kobayashi, R.; Normand, J.; Raghavachari, K.; Rendell, A. P.; Burant, J. C.; Iyengar, S. S.; Tomasi, J.; Cossi, M.; Millam, J. M.; Klene, M.; Adamo, C.; Cammi, R.; Ochterski, J. W.; Martin, R. L.; Morokuma, K.; Farkas, O.; Foresman, J. B.; Fox, D. J. Gaussian 16, Revision C.01. 2016, Gaussian, Inc.: Wallingford CT.

(42) Lee, C.; Yang, W.; Parr, R. G. Development of the Colle-Salvetti Correlation-Energy Formula into a Functional of the Electron Density. *Phys. Rev. B* **1988**, *37*, 785−789.

(43) Becke, A. D. Density-functional Thermochemistry. III. The Role of Exact Exchange. *J. Chem. Phys.* **1993**, *98*, 5648−5652.

(44) Francl, M. M.; Pietro, W. J.; Hehre, W. J.; Binkley, J. S.; Gordon, M. S.; DeFrees, D. J.; Pople, J. A. Self-consistent Molecular Orbital Methods. XXIII. A Polarization-type Basis Set for Second-row Elements. *J. Chem. Phys.* **1982**, *77*, 3654−3665.

(45) Hehre, W. J.; Ditchfield, R.; Pople, J. A. Self-Consistent Molecular Orbital Methods. XII. Further Extensions of Gaussian-Type Basis Sets for Use in Molecular Orbital Studies of Organic Molecules. *J. Chem. Phys.* **1972**, *56*, 2257−2261.

(46) Frisch, M. J.; Pople, J. A.; Binkley, J. S. Self-consistent Molecular Orbital Methods 25. Supplementary Functions for Gaussian Basis Sets. *J. Chem. Phys.* **1984**, *80*, 3265−3269.

(47) Watson, J.; Santaloci, T. J.; Cheema, H.; Fortenberry, R. C.; Delcamp, J. H. Full Visible Spectrum Panchromatic Triple Donor Dye for Dye-Sensitized Solar Cells. *J. Phys. Chem. C* **2020**, *124*, 25211−25220.

(48) SnO$_2$ Transparent Printing Pastes from Powders for Photon Conversion in SnO$_2$-Based Dye-Sensitized Solar Cells.

(49) Cheema, H.; Watson, J.; Shinde, P. S.; Rodrigues, R. R.; Pan, S.; Delcamp, J. H. Precious Metal-Free Solar-to-Fuel Generation: SSM-DSCs Powering Water Splitting with NanoCOT and NiMoZn Electrocatalysts. *Chem. Commun.* **2020**, *56*, 1569−1572.

(50) Franchi, D.; Calamante, M.; Reginato, G.; Zani, L.; Peruzzini, M.; Taddei, M.; Fabrizi de Biani, F.; Basosi, R.; Sinicropi, A.; Colonna, D.; Di Carlo, A.; Mordini, A. A Comparison of Carboxypyridine Isomers as Sensitizers for Dye-Sensitized Solar Cells: Assessment of Device Efficiency and Stability. *Tetrahedron* **2014**, *70*, 6285−6295.

(51) Liu, J.; Zhou, D.; Xu, M.; Jing, X.; Wang, P. The Structure−Property Relationship of Organic Dyes in Mesoscopic Titania Solar Cells: Only One Double-Bond Difference. *Energy Environ. Sci.* **2011**, *4*, 3545.

(52) Furube, A.; Katoh, R.; Hara, K.; Sato, T.; Murata, S.; Arakawa, H.; Tachiya, M. Lithium Ion Effect on Electron Injection from a Photoexcited Coumarin Derivative into a TiO$_2$ Nanocrystalline Film Investigated by Visible-to-IR Ultrafast Spectroscopy. *J. Phys. Chem. B* **2005**, *109*, 16406−16414.

(53) Durrant, J. R.; Haque, S. A.; Palomares, E. Towards Optimisation of Electron Transfer Processes in Dye Sensitised Solar Cells. *Coord. Chem. Rev.* **2004**, *248*, 1247−1257.

(54) Fredin, K.; Nissfolk, J.; Boschloo, G.; Hagfeldt, A. The Influence of Cations on Charge Accumulation in Dye-Sensitized Solar Cells. *J. Electroanal. Chem.* **2007**, *609*, 55−60.

(55) Koops, S. E.; O'Regan, B. C.; Barnes, P. R. F.; Durrant, J. R. Parameters Influencing the Efficiency of Electron Injection in Dye-Sensitized Solar Cells. *J. Am. Chem. Soc.* **2009**, *131*, 4808−4818.

(56) Nakade, S.; Kanzaki, T.; Kubo, W.; Kitamura, T.; Wada, Y.; Yanagida, S. Role of Electrolytes on Charge Recombination in Dye-Sensitized TiO$_2$ Solar Cell (1): The Case of Solar Cells Using the I$^-$/I$_3^-$ Redox Couple. *J. Phys. Chem. B* **2005**, *109*, 3480−3487.

(57) Haque, S. A.; Tachibana, Y.; Willis, R. L.; Moser, J. E.; Grätzel, M.; Klug, D. R.; Durrant, J. R. Parameters Influencing Charge Recombination Kinetics in Dye-Sensitized Nanocrystalline Titanium Dioxide Films. *J. Phys. Chem. B* **2000**, *104*, 538−547.

(58) Ito, S.; Miura, H.; Uchida, S.; Takata, M.; Sumioka, K.; Liska, P.; Comte, P.; Péchy, P.; Grätzel, M. High-Conversion-Efficiency Organic Dye-Sensitized Solar Cells with a Novel Indoline Dye. *Chem. Commun.* **2008**, 5194−5196.

(59) Meador, W. E.; Liyanage, N. P.; Watson, J.; Groenhout, K.; Delcamp, J. H. Panchromatic NIR-Absorbing Sensitizers with a Thienopyrazine Auxiliary Acceptor for Dye-Sensitized Solar Cells. *ACS Appl. Energy Mater.* **2023**, *6*, 5416−5428.

(60) Houle, F. A. Adaptive Response by an Electrolyte: Resilience to Electron Losses in a Dye-Sensitized Porous Photoanode. *Chem. Sci.* **2021**, *12*, 6117−6128.

(61) Tiwana, P.; Docampo, P.; Johnston, M. B.; Herz, L. M.; Snaith, H. J. The Origin of an Efficiency Improving "Light Soaking" Effect in SnO2 Based Solid-State Dye-Sensitized Solar Cells. *Energy Environ. Sci.* **2012**, *5*, 9566.

(62) Raithel, A. L.; Meador, W. E.; Kim, T.-Y.; Staples, R. J.; Delcamp, J. H.; Hamann, T. W. Molecular Switch Cobalt Redox Shuttle with a Tunable Hexadentate Ligand. *J. Am. Chem. Soc.* **2023**, *145*, 1367−1377.

(63) Boschloo, G.; Häggman, L.; Hagfeldt, A. Quantification of the Effect of 4-*Tert*-Butylpyridine Addition to I$^-$/I$_3^-$ Redox Electrolytes in Dye-Sensitized Nanostructured TiO$_2$ Solar Cells. *J. Phys. Chem. B* **2006**, *110*, 13144−13150.